Comparison of a Separated Flow Response to Localized and Global-type Disturbances

Monnier, B.; Williams, D. R.; Weier, T.; Albrecht, T.;

Originally published:

June 2016

Experiments in Fluids 57(2016), 114

DOI: https://doi.org/10.1007/s00348-016-2199-4

Noname manuscript No.
(will be inserted by the editor)

Comparison of a Separated Flow Response to Localized and Global-type Disturbances

Bruno Monnier · David R. Williams · Tom Weier · Thomas Albrecht

Received: date / Accepted: date

Abstract The flow structure and lift response of a separated flow over an airfoil that is subjected to an impulsive type of pitching motion is compared to the response produced by a localized pulse disturbance at the leading edge of an airfoil. Time-resolved PIV data is used to obtain the velocity field on the suction surface of the airfoil. POD analysis shows that the majority of energy is contained within the first four modes. Strong similarities in the shapes of the POD basis functions are found, irrespective of the type of actuation (global or local). The time-varying coefficient of the second POD mode tracks the negative of the lift coefficient in each case. Basis functions from the localized actuation data were projected on the velocity field of the globally actuated flow to obtain a hybrid set of coefficients. The hybrid coefficients matched reasonably well with the coefficients obtained from the original POD analysis for the globally excited flow. Both types of actuation were found to generate very similar Lagrangian flow structures. The results suggest a certain degree of universality in the POD modes/flow structures for the separated flow over an airfoil, irrespective of the type of excitation.

1 INTRODUCTION

The ability to model the response of a separated flow to external disturbances is an important component in the design of active flow control systems. Full Navier-Stokes simulations are generally too slow to be useful in real-time control systems,

B. Monnier · D.R. Williams
Department of Mechanical, Materials and Aerospace Engineering, Illinois Institute of Technology, Chicago, Illinois, USA
E-mail: {bmonnier, williamsd}@iit.edu

T. Weier
Helmholtz-Zentrum Dresden - Rossendorf, Bautzner Landstr. 400, 01328 Dresden, Germany
E-mail: T.weier@hzdr.de

T. Albrecht
Department of Mechanical and Aerospace Engineering, Monash University, VIC 3800, Australia,
E-mail: thomas.albrecht@monash.edu

so we look for reduced-order models that can run much faster and still reproduce the flow characteristics relevant to the control problem under consideration. Low-dimensional models that capture the separated flow response to actuator input (a.k.a. plant models) are useful in the design of feedback controllers, while models that describe the flow's response to large-scale external disturbances, such as, gusts or angle of attack changes are used in the design of both feed back and feed forward controllers (Kerstens et al, 2011).

The development of effective low-dimensional models often benefits from some insight into the underlying flow physics. Evidence that separated flow dynamics may be controlled by only a few instability mechanisms was obtained by Raju et al (2008), who used two-dimensional numerical simulations to solve the unsteady, viscous, and compressible Navier-Stokes equations. They identified three distinct time scales associated with the separated flow region, which we can assume are the result of instability modes that govern the dynamic response to disturbances. The three time scales are connected with the separating shear layer at the leading edge, the separation bubble, and the wake behind the airfoil. Spatially localized (near the leading edge of the airfoil), periodic zero-net-mass-flux excitation was used to provide a continuous input signal to the separated flow, which enabled the identification of the three distinct time scales. One expects that the dynamics governing those three modes will be independent from the type of disturbance input, but the output flow response will depend on both the spatial and temporal details of the input signal.

The spatial dimensions of most active flow control actuators are usually small compared to the characteristic length scale of the test article. As a result only the time varying component of actuation is considered, i.e., the actuator may be producing a sinusoidal, square-wave, triangle, or burst type of actuation. However, in the case of the pitching airfoil, the entire chord of the airfoil is perturbing the flow so the actuator has a large spatial dimension. Both the spatial distribution of the actuator and its temporal signal are expected to affect the flow field response. A single pulse-type of input disturbance will introduce a broader band frequency spectrum than a continuous, periodically driven signal at a single frequency. Similarly, a spatially localized input signal would have a broader band in the wave number spectrum than a large-scale disturbance produced by the motion of the airfoil.

In this paper we chose to use a single pulse as the temporal component disturbance input, because it introduces a finite amount of energy into the separated flow. Furthermore, for very short duration input pulses, the response approaches the impulse response function that can be used to model linear systems. The effect of spatially localized disturbances introduced into the separated flow region on an airfoil were investigated by Albrecht et al (2015) for the case of a stationary airfoil. The length scale of the actuator was only 3.8 percent of the chord length. By contrast, the entire airfoil can produce a spatially distributed disturbance to the separated flow by rapidly pitching the airfoil with a small amplitude, pitch-up/pitch-down pulse-type maneuver. In the latter case, the entire chord of the airfoil defines the length scale of the actuator. Clearly the initial conditions for the two disturbances are significantly different, and we can expect the effects on the flow field will be different. For example, the pitch-pulse maneuver may produce both leading and trailing edge vortices, but the localized pulse from a Lorentz force actuator will only affect the region close to the actuator. However, in the

long term, both flows will return to the same initially undisturbed, separated flow condition. In this work we examine the similarities and differences between the dynamics of the separated flow region with the two types of actuation.

To better quantify the effects of actuation, the snapshot proper orthogonal decomposition (POD) method introduced by Sirovich (1987) is used to identify the dominant spatial modes and the temporal coefficients of the flow field response to the different input disturbances. The effect of the different input disturbances on the POD mode shapes and the temporal coefficients is examined. Furthermore, both positive and negative types of actuation are examined. Here 'positive/negative' refers to the direction of the pulse. In the case of the Lorentz force actuator, the force may be directed in either the downstream or upstream direction. For the pitching airfoil case, the disturbance pitch angle can be either increased or decreased relative to the static angle of attack.

The experimental conditions for the Lorentz force actuator and the pitching airfoil are provided in section 2. Results of the POD analysis, low order representation and lift relationship for the localized disturbance (Lorentz force) and the global disturbance (pitching airfoil) are given in section 3. Finite time Lyapunov exponent analysis (FTLE, see Shadden et al (2005)) is used to compare the Lagrangian flow structures with the POD modes in section 4. Conclusions obtained by the comparisons are provided in section 5.

2 EXPERIMENTAL PROCEDURE

Two types of actuation were used, a spatially localized pulse created with a Lorentz force actuator near the leading edge, and a global disturbance created by pitching an airfoil through a two degree change in angle of attack. In both cases, the sign of the disturbance could be changed. With Lorentz force actuation the direction of the disturbance could be either downstream (positive disturbance), or against the flow (negative disturbance). In the case of the pitching airfoil, the angle of attack could increase suddenly (positive disturbance) and then come back the baseline angle, or decrease suddenly (negative disturbance) and come back the baseline angle. To compare the timing of both types of actuation, we introduce t^+, which is a dimensionless parameter based on the convective time scale and defined as $\frac{tU_\infty}{c}$, where t is time in seconds, U_∞ is the mean freestream velocity and c is the chord of the airfoil under consideration. In both cases, the actuation occurs at $t^+ = 0$ and temporal data is presented from $t^+ = -1$ to about $t^+ = 8 - -9$.

2.1 Localized disturbance experiments

The localized actuator experiments were conducted in the small electrolyte channel at the Helmholtz-Zentrum Dresden-Rossendorf. The facility has a free surface test section with cross section dimensions 0.2×0.2 m and a length of 1 m. A settling chamber, honeycomb, and screens reduce the freestream turbulence level in the test section to approximately 1 percent. The separated flow region was produced by a flat plate with a rounded leading edge inclined at $\alpha = 16^\circ$ with respect to the incoming flow. The plate was made from acrylic glass enabling a laser light sheet to illuminate both sides of the body, except for small regions on the pressure

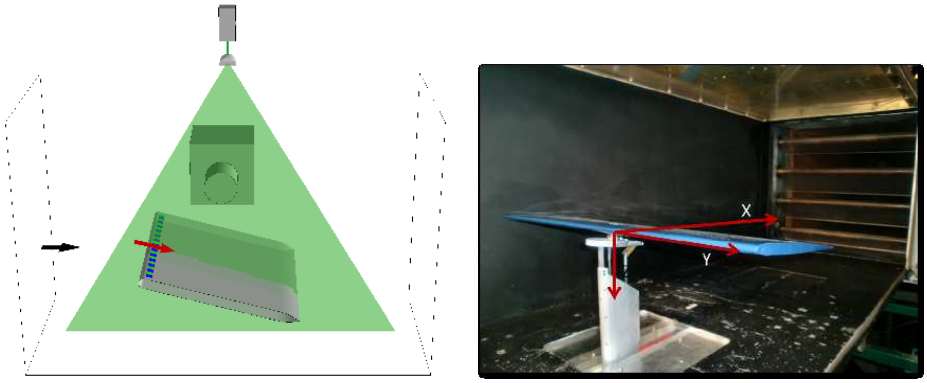

(a) PIV orientation (b) NACA 0009 airfoil

Fig. 1 Experimental setup - a) orientation of flat plate and laser light sheet used for PIV measurements in the Dresden NaOH channel. b) NACA 0009 airfoil in the IIT wind tunnel with the coordinate system.

side of the airfoil where the opaque actuator blocked the light. The chord length of the model was $c = 0.130$ m. A schematic of this experimental setup is shown in Figure 1(a).

The freestream speed through the channel was $U_\infty = 0.08$ m/s, which produced a chord Reynolds number $Re = 10{,}000$. Velocity field data was obtained with a two-dimensional, two-component, time-resolved PIV system. The PIV system acquired data at 60 frames per second. The actuation Data recording began at $t^+ = -1$ before the pulse, and continued until $t^+ = 9$ after the pulse.

Actuation of the flow, at $t^+ = 0$, was done with a set of electro-magnetic actuators mounted near the leading edge of the airfoil. These are represented schematically in Figure 2. The actuator length is $a = 5$ mm ($0.0385\,c$). Because the fluid is electrically conducting, a Lorentz force generated by non-parallel electric and magnetic fields produces a body force on the fluid that is capable of reattaching a separated flow under steady state conditions (Cierpka et al, 2008, 2010). The Lorentz force density $\boldsymbol{f} = \boldsymbol{j} \times \boldsymbol{B}$ acting on the flow is directly proportional to the electric current density $\boldsymbol{j}$ and the magnetic induction $\boldsymbol{B}$. Hence, we obtain arbitrary time signals of the force by simply modulating the electric current. For the given magnetic induction magnitude $B_0 = 0.4$ T and electric conductivity $\sigma = 0.5$ S/m, the Lorentz force can be shown to be independent of the flow speed. The Lorentz force actuators have very high bandwidth and independently controllable amplitude and frequency. As discussed by Cierpka et al (2010), the Lorentz force actuators provide momentum without an associated mass flux. The bandwidth is effectively unlimited, and arbitrary waveforms can be chosen. A square-wave type pulse with a short duty cycle was used to excite the separated shear layer. The short pulse repeated every $t^+ = 20$ to allow the flow time to re-establish its undisturbed state. In this paper, we investigate an upstream and downstream pulse with duration $\Delta t^+ = 0.1$ and rms momentum coefficient $C'_\mu = 0.11\%$ (see Albrecht et al (2015) for more information about flow dependence on pulse magnitude or width).

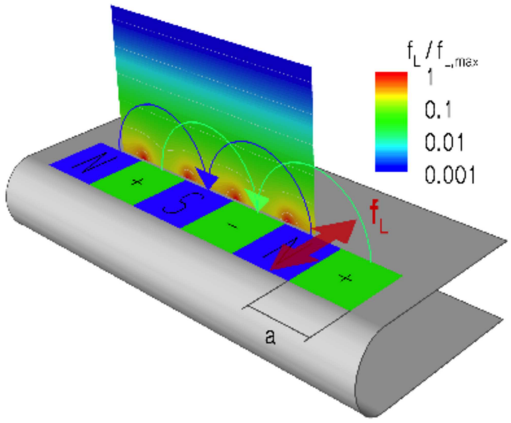

Fig. 2 Lorentz Force.

2.2 Global disturbance experiments

The pitch-pulse experiments were conducted at the Illinois Institute of Technology, Fejer Unsteady Flow Wind Tunnel. The cross sectional dimensions of the test section are 600 mm × 600 mm, and it has a length of 3.1 m. The test article shown in Figure 1(b) is a two-dimensional airfoil with an NACA 0009 profile (c = 245 mm, S = 600 mm), which spans the width of the wind tunnel test section. There is a 2 mm gap between the airfoil and the sidewalls of the wind tunnel to allow the airfoil to pitch without interference from the side walls. The freestream speed was $U_\infty = 3$ m/s, which gave a chord based Reynolds number $Re_c = 57{,}000$. At 3 m/s the turbulence level of the freestream velocity is 0.6 percent over a band from 0.1 Hz to 30 Hz.

In analog to the localized Lorentz force disturbance, the separated flow over an airfoil was disturbed with two signs of pitching maneuvers about the quarter chord. The positive pitch–up maneuver started at 15°, pitched up to 17°, then pitched down to 15°. The negative pitch–down maneuver was from 15° to 13°, back to 15°. These maneuvers were controlled by displacing the back rod holding the airfoil in place in the wind tunnel (see Figure 1(b)). This rod is connected to a linear magnetic motor and the position can be recorded via the integrated encoder. The commanded step pitch maneuvers, at $t^+ = 0$, and recorded actual angles of attack are shown in Figure 3. The maximum amplitude of the step pitch maneuver is attained in about half a convective time and it takes about another half a convective time to come back to the baseline angle, yielding $\Delta t^+ \approx 1$. The step pitch maneuvers are therefore about 10 times longer than the localized pulse experiments.

Velocity field data was obtained with a two-dimensional, two-component PIV system. The PIV system acquired data at 5 frames per second not allowing for time resolved data. Therefore, the data was phase averaged and resulted in 96 phases covering a range of $t^= - 1$ to about $t^+ = 8$. For each phase, 80 cycles of the step pitch maneuver were averaged. A sufficient amount of time was allowed

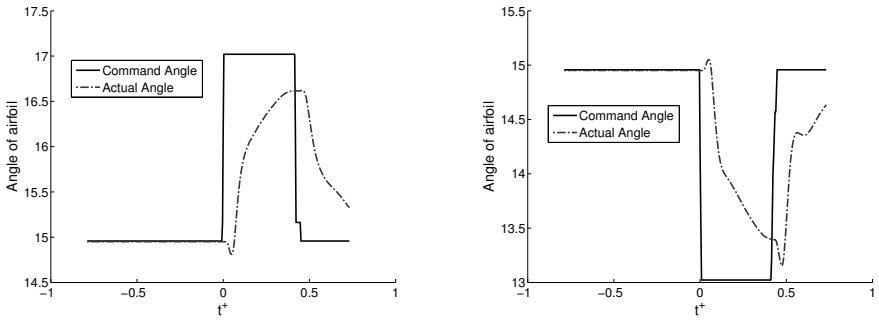

(a) Global disturbance, pitch up (b) Global disturbance, pitch down

Fig. 3 Angular position of the airfoil versus t^+.

to pass between the recording of each cycle to so that the flow could readjust to its steady state baseline.

3 LOW ORDER REPRESENTATION AND LIFT RELATIONSHIP

3.1 POD analysis

The localized disturbance experiments described previously (both positive and negative) as well as the global disturbance experiments (step pitch up and down) constitute the four data sets that are investigated in this paper. Sample instantaneous velocity fields at $t^+ = 1$ from each of them are presented in Figure 4. It is important to note that all data sets are normalized by the chord length of the corresponding airfoil and that they are carefully matched to cover the same spatial extent. In other words, only data in a fixed common spatial domain is considered for the POD analysis. The spatial domain delimited by the moving boundary of the pitching airfoil data sets is therefore not included.

The POD method, see equation 1, is then applied to each complete set of velocity field data in the expectation of gaining additional insight into the details of the flow structure.

$$\boldsymbol{V}(\boldsymbol{x},t) = \sum_{i=1}^{n} \zeta_i(t)\boldsymbol{\psi}_i(\boldsymbol{x}) \tag{1}$$

The 2-dimensional velocity field (streamwise and wall normal components) $\boldsymbol{V}(\boldsymbol{x},t)$ is decomposed in a set of temporal POD coefficients $\zeta_i(t)$ and normalized spatial POD basis functions $\boldsymbol{\psi}_i(\boldsymbol{x})$. The number of snapshots, n, used to perform the POD decomposition was 96 for the global disturbance data sets (step pitch) and 968 for the localized disturbance data sets.

Using the POD coefficients, the normalized mode energy distributions for the two types of disturbances (local and global) are calculated and presented in Figure 5. The mode energy drops quickly, suggesting that the important dynamics of the separated flow response to a single pulse could be captured reasonably well with only a few POD modes. The upstream directed pulse distributes more of its

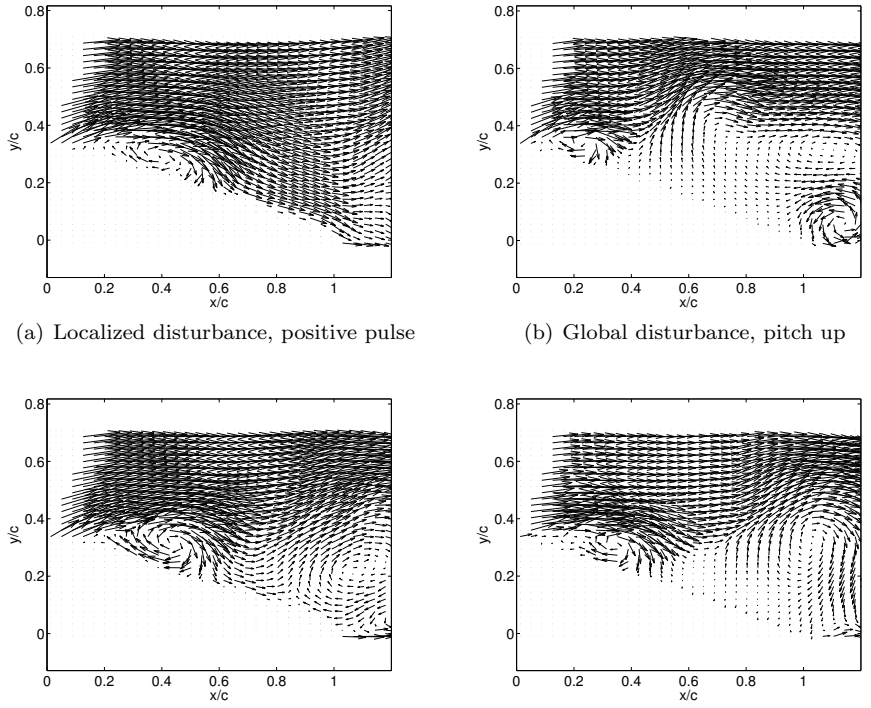

(a) Localized disturbance, positive pulse

(b) Global disturbance, pitch up

(c) Localized disturbance, negative pulse

(d) Global disturbance, pitch down

Fig. 4 Sample instantaneous velocity field at $t^+ = 1$.

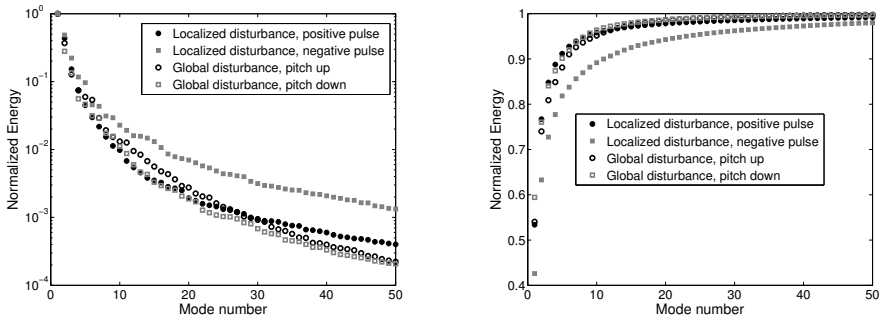

(a) Normalized energy

(b) Cumulative normalized energy

Fig. 5 Energy distribution versus mode number.

energy over the higher modes than the downstream directed pulse, but significant differences in mode energy do not appear until the 3$^{\text{rd}}$ mode and higher.

3.2 Low order comparison of both types of actuation

Figures 6 and 7 present a side by side comparison of the first two POD modes associated with the localized disturbance data sets and the global disturbance data sets. The left column shows the POD basis functions for the positive/negative pulse data and the right column shows the corresponding pitch up/down cases.

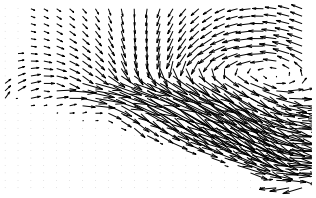

(a) Localized disturbance, positive pulse Mode 1, $\boldsymbol{\psi}_1(x)$

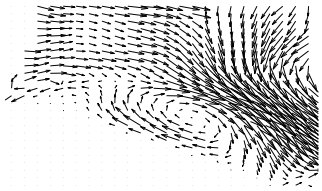

(b) Global disturbance, pitch up Mode 1, $\boldsymbol{\psi}_1(x)$

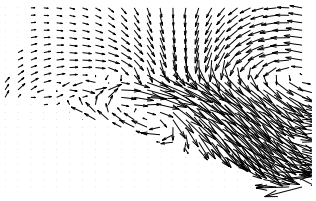

(c) Localized disturbance, negative pulse Mode 1, $\boldsymbol{\psi}_1(x)$

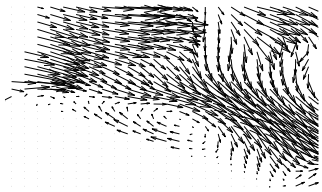

(d) Global disturbance, pitch down Mode 1, $\boldsymbol{\psi}_1(x)$

Fig. 6 Comparison side by side for POD mode 1 – positive/negative pulse (left) and pitch up/down (right).

In general, strong similarities in Modes 1 and 2 are observed and the structure of all four cases contain two counter-rotating vortices; however, the positions of these vortices relative to the airfoil are somewhat dependent on the type and direction of actuation.

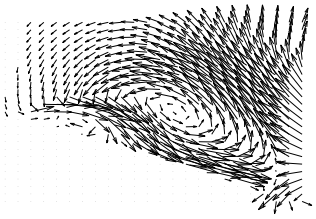

(a) Localized disturbance, positive pulse Mode 2, $\psi_2(x)$

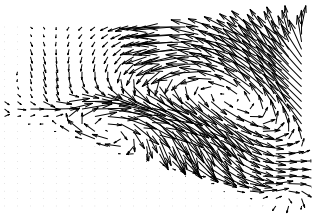

(b) Global disturbance, pitch up Mode 2, $\psi_2(x)$

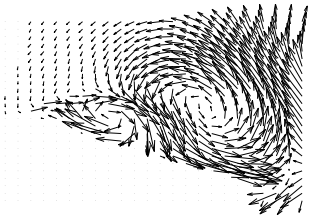

(c) Localized disturbance, negative pulse Mode 2, $\psi_2(x)$

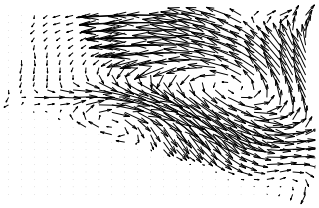

(d) Global disturbance, pitch down Mode 2, $\psi_2(x)$

Fig. 7 Comparison side by side for POD mode 2 – positive/negative pulse (left) and pitch up/down (right).

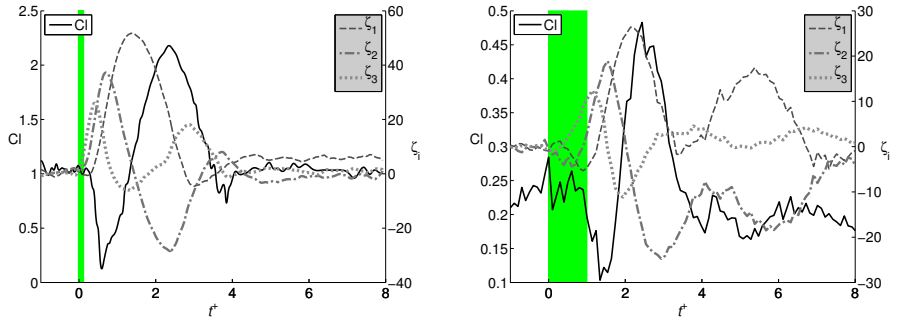

(a) Localized disturbance for positive pulse (b) Global disturbance for step pitch up $15° - 17° - 15°$

Fig. 8 Hybrid POD coefficients associated with modes 1, 2 and 3 and lift coefficient vs. t^+.

3.3 Hybrid POD coefficients

The strong similarities observed in the spatial POD modes obtained for all four data sets motivates the study presented in this section. For control systems, a universal set of spatial basis functions that would be applicable to a wide range of actuation types would be highly desirable.

From here on, we only use POD basis functions associated with a single data set (localized disturbance, positive pulse, $\boldsymbol{\psi}_{i,\mathrm{local}+}$) for our calculations. Hybrid POD coefficients are then calculated for all four data sets using these basis functions as:

$$\zeta_i(t) = \int_\Omega \boldsymbol{V}(\boldsymbol{x},t)\boldsymbol{\psi}_{i,\mathrm{local}+}(\boldsymbol{x})\mathrm{d}\boldsymbol{x} \tag{2}$$

The first three hybrid coefficients associated with the localized disturbance positive pulse and the global disturbance pitch up are presented in Figure 8 along with the corresponding lift coefficient as a function of t^+. The green shaded rectangles represent the beginning and duration of both types of actuation. In Figure 8(a) presenting results for a localized disturbance, the lift coefficient was derived from the measured velocity field (using data from all around the airfoil) using the momentum equation in integral form (see Albrecht et al (2015) and Unal et al (1997) for more details on the technique). In Figure 8(b) presenting the results for a global disturbance, the lift coefficient is only a rough estimate based on the available data from the suction side of the airfoil by performing integration of the circulation.

These hybrid coefficients provide information about the strength (and importance) of the various spatial modes during the transient response to a pulse from the actuator. The data in Figure 8(a) show the coefficients for the first three POD modes superposed with the lift coefficient. Positive values of temporal coefficients for modes 1 and 3 contribute to enhanced lift, while a positive value of the 2^{nd} mode coefficient acts to reduce the lift. Mode 2 changes sign and reaches its strongest negative value near $t^+ = 2.5$ when the lift increment reaches its peak. The negative of the mode 2 temporal coefficient closely tracks the overall lift coefficient, which might be useful in future flow control applications. The coefficients shown

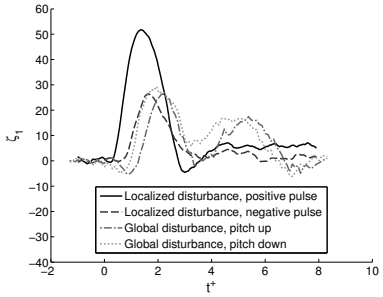

(a) Mode 1 POD coefficient, ζ_1

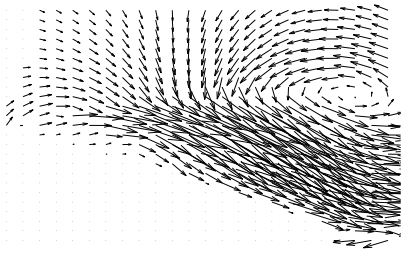

(b) Mode 1 POD basis function, $\psi_{1,\mathrm{local}+}$

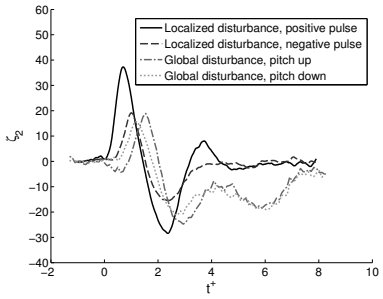

(c) Mode 2 POD coefficient, ζ_2

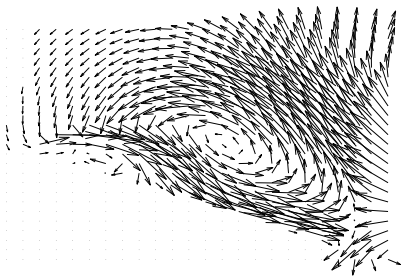

(d) Mode 2 POD basis function, $\psi_{2,\mathrm{local}+}$

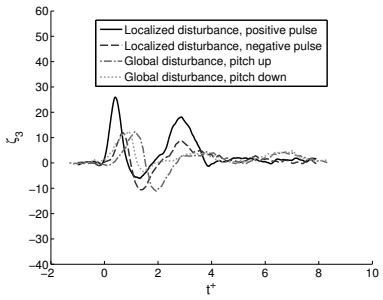

(e) Mode 3 POD coefficient, ζ_3

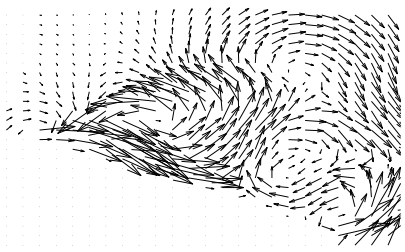

(f) Mode 3 POD basis function, $\psi_{3,\mathrm{local}+}$

Fig. 9 Velocity POD coefficients associated with modes 1, 2 and 3 for all four cases and corresponding basis functions.

in Figure 8(b) display a similar relationship with the lift coefficient (estimated by integration of the circulation around the airfoil).

This motivates the next series of graphs that present a comparison of the temporal evolution of the hybrid POD coefficients associated with the first four modes, shown in Figures 9 and 10. The corresponding POD basis functions used to calculate the hybrid POD coefficients are shown in the right column. Overall, the temporal evolution of the hybrid POD coefficients seem to follow the same patterns for all four data sets although some differences are notable. For the first three modes (Figures 9(a) through 9(f)), the positive pulse data set clearly displays

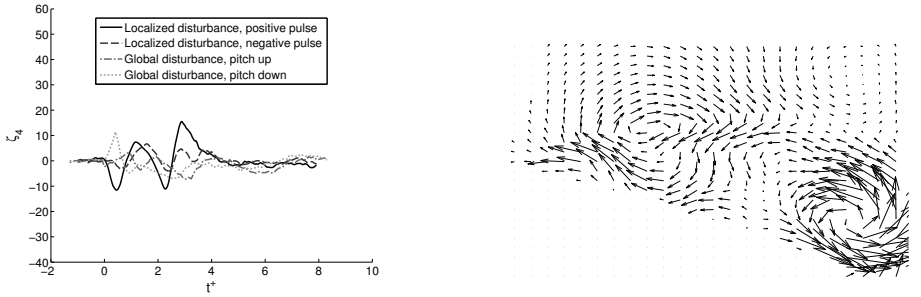

(a) Mode 4 POD coefficient, ζ_4

(b) Mode 4 POD basis function, $\psi_{4,\text{local}+}$

Fig. 10 Velocity POD coefficients associated with mode 4 for all four cases and corresponding basis functions.

a quicker response in the sense that the associated hybrid POD coefficients reach a peak sooner than the hybrid POD coefficients associated with the other data sets. The time at which this peak is reached, denoted as t_r^+, is akin to a time response. Using this definition, Table 1 summarizes the time response, t_r^+, for each data set and POD modes up to mode 3. The data sets are ordered from quickest to slowest to reach the peak value of their respective first POD coefficient. Incidentally, the other two modes follow the same trends.

The same test was repeated with a different set of reference spatial basis functions, $\boldsymbol{\psi}_{i,\text{local}-}(\boldsymbol{x})$, associated with the localized disturbance negative pulse data set and the same observations still hold true. The fact that the order is the same for the first three modes indicates that the response to the disturbance for the positive pulse is indeed quicker. Then come the negative pulse, pitch down and finally pitch up data sets. This is in agreement with observation of the timing of the formation of flow structures for the different data sets based on FTLE fields presented in section 4.

Table 1 Time response t_r^+ measured as t^+ at which a POD coefficient reaches its first peak.

Data set	Mode 1 t_r^+	Mode 2 t_r^+	Mode 3 t_r^+
Positive pulse	1.37	0.70	0.41
Negative pulse	1.64	1.00	0.68
Pitch down	1.94	1.14	0.90
Pitch up	2.14	1.54	1.14

Another difference between the two types of actuation is the secondary increase of the hybrid POD coefficients associated with the pitched airfoil (essentially ζ_1 and ζ_2 for $4.0 < t^+ < 6.5$, see Figures 9(a) and 9(c)), which is absent in the localized disturbance cases. Finally, hybrid POD coefficients associated with the fourth mode, presented in Figure 10(a), show no common temporal behavior. This is not surprising as this mode captures essentially a vortical structure near the trailing edge of the airfoil (see Figure 10(b).) As noted earlier, the pitch up/down maneu-

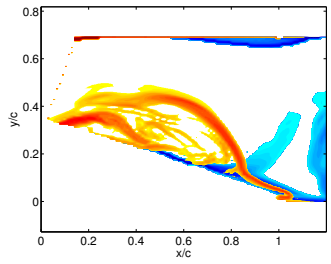

(a) Localized disturbance, positive pulse, $t_r^+ = 1.37$

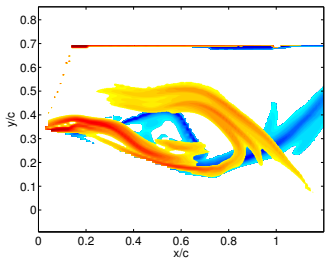

(b) Global disturbance, pitch up, $t_r^+ = 2.14$

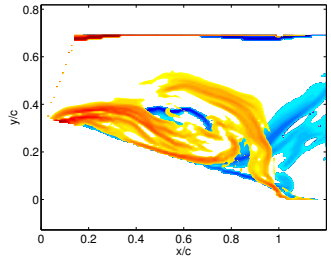

(c) Localized disturbance, negative pulse, $t_r^+ = 1.64$

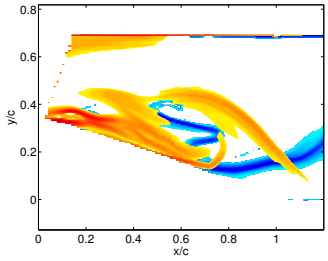

(d) Global disturbance, pitch down, $t_r^+ = 1.94$

Fig. 11 FTLE fields at t_r^+ for Mode 1.

vers are generating trailing edge vortices that are not observed in the localized disturbance positive/negative pulse data sets.

4 FLOW STRUCTURES CAPTURED BY FTLE FIELDS

As mentioned earlier with the POD coefficients discussion, the timing of the flow response is slightly different between the four data sets. In order to have a more comprehensive comparison between the different types of actuation, we use again the definition of time response with respect to the peaks in the POD coefficients, t_r^+, introduced previously.

Figure 11 shows instantaneous snapshots of the FTLE fields associated with the four data sets. Positive time integration is displayed as a yellow to red color gradient while negative time integration is displayed as a light to dark blue color gradient. The particular instant that is displayed corresponds to the t^+ at which their respective POD coefficient associated with Mode 1 is at its first peak (defined earlier as t_r^+, see Figure 9(a) for the coefficients and Table 1 for values). At this instant in time, the FTLE fields for each data sets show very strong similarities in the flow structure. Essentially, a large vortical structure occupying most of the suction side of the airfoil is present in all four cases.

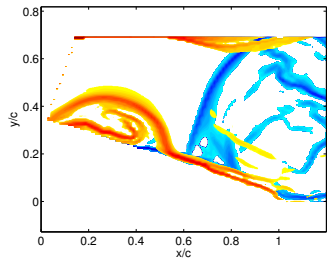

(a) Localized disturbance, positive pulse, $t_r^+ = 0.70$

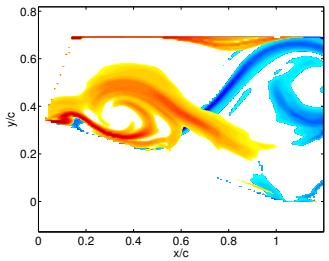

(b) Global disturbance, pitch up, $t_r^+ = 1.54$

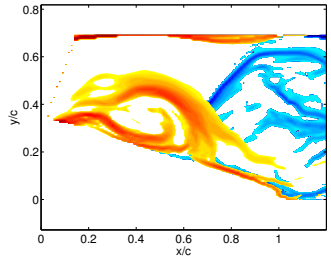

(c) Localized disturbance, negative pulse, $t_r^+ = 1.00$

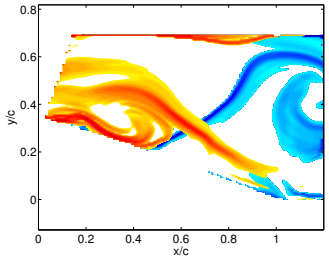

(d) Global disturbance, pitch down, $t_r^+ = 1.14$

Fig. 12 FTLE fields at t_r^+ for Mode 2.

Figures 12 and 13 present the same type of results at t_r^+ of Modes 2 and 3, respectively. As seen in Table 1, t_r^+ of Mode 2 is shorter than the one of Mode 1. Therefore the snapshots of FTLE presented in Figure 12 show the flow structure at an earlier time. The large vortical structure observed at t_r^+ of Mode 1 is smaller in size and located closer to the leading edge of the airfoil. This corresponds to the leading edge vortex (LEV) shed after a disturbance is introduced in the flow field. Finally, for t_r^+ of Mode 3 which is at an even earlier time, the LEV is again smaller in size and closer to the leading edge of the airfoil. Again, the agreement in flow structures between the four data sets is very good at the two t_r^+ shown in Figures 12 and 13.

5 SUMMARY

A comparison of the structures of velocity field POD modes that result from a separated flow over an airfoil show strong similarities irrespective of the type of disturbance. Spatially localized disturbances created by a Lorentz force actuator produce POD modes and FTLE flow structures that are quite similar to those produced by a global type of disturbance when the entire airfoil is suddenly pitched through a small angle. In both cases it is shown that the temporal coefficient of

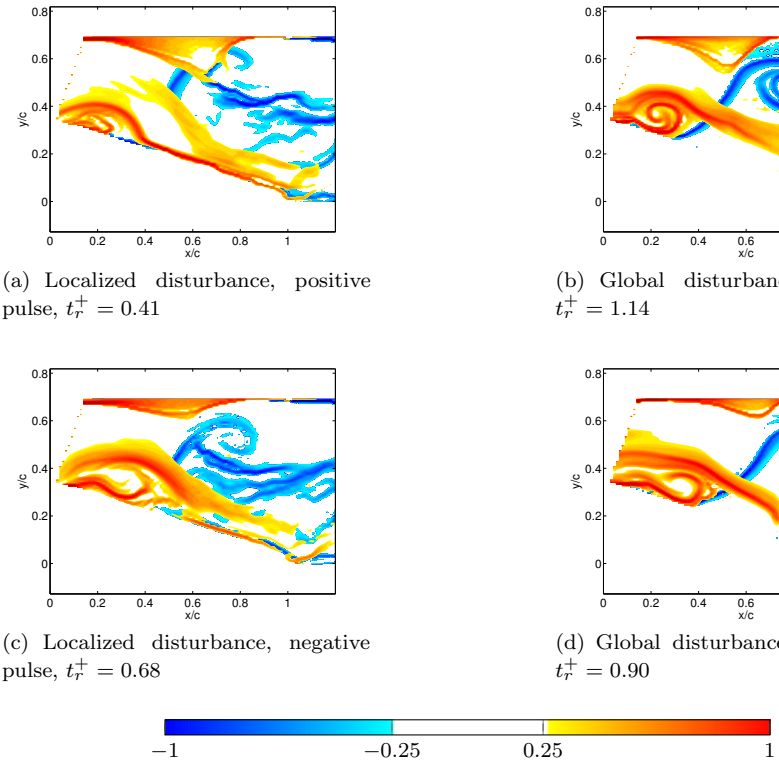

(a) Localized disturbance, positive pulse, $t_r^+ = 0.41$

(b) Global disturbance, pitch up, $t_r^+ = 1.14$

(c) Localized disturbance, negative pulse, $t_r^+ = 0.68$

(d) Global disturbance, pitch down, $t_r^+ = 0.90$

Fig. 13 FTLE fields at t_r^+ for Mode 3.

the second POD mode tracks the negative of the lift coefficient reasonably well, which may be useful for future flow control applications. The structures identified using FTLE analysis correlate well with the first three POD mode basis functions at the time that each specific mode is dominant in its amplitude.

Differences between the local and global actuation were most prominent in the first POD mode. A secondary increase in mode amplitude was observed for the pitched airfoil, between $4.0 < t^+ < 6.5$, which was absent for Lorentz force actuation on the stationary airfoil. The times for the peak amplitudes to be reached were significantly different for all types of actuation. The localized downstream disturbance showed the fastest response, with the first three modes reaching their peak amplitude about twice as fast as compared with the positive pitching airfoil case.

ACKNOWLEDGMENT

Support for Bruno Monnier and David R. Williams from the U.S. Air Force Office of Scientific Research (FA9550-12-1-0075) with program manager Dr. Douglas Smith is gratefully acknowledged.

References

Albrecht T, Weier T, Gerbeth G, Monnier B, Williams DR (2015) Separated flow response to single pulse actuation. AIAA Journal 53(1):190–199

Cierpka C, Weier T, Gerbeth G (2008) Evolution of vortex structures in an electromagnetically excited separated flow. Experiments in Fluids 45:943–953

Cierpka C, Weier T, Gerbeth G (2010) Synchronized force and particle image velocimetry measurements on an naca 0015 in poststall under control of time periodic electromagnetic forcing. Physics of Fluids 22(075109)

Kerstens W, Williams D, Pfeiffer J, King R, Colonius T (2011) Closed-loop control of lift for longitudinal gust suppression at low reynolds numbers. AIAA Journal 49(8):1721–1728

Raju R, Mittal R, Cattafesta L (2008) Dynamics of airfoil separation control using zero-net-mass-flux forcing. AIAA Journal 46(12):3103–3115

Shadden S, Lekien F, Mardsen J (2005) Definition and properties of lagrangian coherent structures from finite-time lyapunov exponents in two-dimensional aperiodic flows. Physica D 212(3–4):271–304

Sirovich L (1987) Turbulence and the dynamics of coherent structures, Part I: Coherent structures. Quarterly of Applied Mathematics 45(3):561–571

Unal M, Lin J, Rockwell D (1997) Force prediction by piv imaging: A momentum-based approach. Journal of Fluids and Structures 11(8):965–971